Journal of Solid State Chemistry 181 (2008) 1621–1627

Contents lists available at ScienceDirect

Journal of Solid State Chemistry

journal homepage: www.elsevier.com/locate/jssc

Solid-state chemistry on a surface and in a beaker: Unconventional routes to transition metal chalcogenide nanomaterials

Christopher L. Stender [a], Perumal Sekar [a,1], Teri W. Odom [a,b,*]

[a] Department of Chemistry, Northwestern University, 2145 Sheridan Road, Evanston, IL 60208, USA
[b] Department of Materials Science and Engineering, Northwestern University, 2145 Sheridan Road, Evanston, IL 60208, USA

ARTICLE INFO

Article history:
Received 8 April 2008
Received in revised form
30 May 2008
Accepted 3 June 2008
Available online 5 June 2008

Keywords:
Chemical nanofabrication
Transition metal chalcogenides
Refractory metals
Nanomaterials

ABSTRACT

This article focuses on two different approaches to create nanoscale transition metal chalcogenide materials. First, we used chemical nanofabrication, a combination of top-down patterning and bottom-up solid-state synthesis, to achieve control over the shape, size, and ordering of the patterned nanomaterials. We demonstrated orientational control over nanocrystals within sub-300 nm patterns of MoS_2 and formed free-standing nanostructures of crystalline NiS_2. In addition, crossed line arrays of mixed metal chalcogenide nanostructures were achieved, and TaS_2 nanopatterns were made by the chemical transformation of tantalum oxide templates. Second, we developed a one-pot procedure using molecular precursors to synthesize two-dimensional $NbSe_2$, TaS_2 and $TaSe_2$ nanoplates and one-dimensional $NbSe_2$ wires depending on the relative amount of surfactants in the reaction mixture. Prospects for these transition metal chalcogenide nanomaterials with controlled shapes and morphologies will be discussed.

1. Background

Metal chalcogenide materials are important in a broad range of applications from solar cells [1,2] to catalysts [3,4] to low-friction surfaces [5,6]. In particular, transition metal chalcogenides (TMCs) have demonstrated promise for battery electrode materials [7,8], photovoltaic devices [9], and photocatalysts [10,11]. Reducing the size and controlling the shape of TMCs to nanoscale dimensions has resulted in enhanced properties compared to bulk. For example, fullerene-like TMC nanotubes (e.g. MoS_2, TiS_2, and WS_2) are more air-stable and show a greater loading capacity of Li [12]. Both characteristics are important for battery storage capacity [13]. In addition, HfS_2 nanotubes show photoluminescence that is blue-shifted compared to the bulk [14]. Spherical inorganic fullerene TMC materials, such as WS_2, also demonstrate superior wear resistance and longer lubrication lifetimes compared to TMC powders [13,15]. Hollow MoS_2-nanoparticles can exhibit an order of magnitude lower frictional coefficient than bulk sputtered MoS_2 and are more stable because of their closed cage configuration [16].

Other layered TMC materials, such as TaS_2, $TaSe_2$, and $NbSe_2$, show complex electronic properties such as superconductivity and charge density wave (CDW) behavior [17–20]. In the case of $NbSe_2$, the superconducting transition temperature (T_c) can be reduced by decreasing the number of layers [21]. $NbSe_2$ nanostructures consisting of ca. 12 layers have shown a slight decrease (0.3 K) in T_c [22]. Conversely, TaS_2 nanowires have exhibited an elevated T_c compared to the bulk (0.6–3.4 K) [23]. Confining the size or reducing the dimension of the materials has also facilitated investigations of new mesoscopic phenomena. For example, one-dimensional (1D) chains of TaS_3, $NbSe_3$ and $TaSe_3$ have been especially important in studying CDW behavior in reduced dimensions [24–26]. Nanowires and ribbons made from $NbSe_3$ demonstrate an order of magnitude suppression in the resistivity around the CDW transition temperature compared to bulk $NbSe_3$ from size effects, and wires consisting of less than 2000 chains show insulating behavior at low temperatures (<50 K) [27,28]. Also, in 1D TaS_3 nanostructures, CDWs were responsible for ohmic conduction at low temperatures [29]. Despite the intriguing possibilities of observing quantum-size effects on superconductivity, there are few reports on different synthetic methods to nanoscale diselenide materials [19,20,22,26,30–32].

Using broad classifications, there are three different routes to generate nanoscale TMC materials: (1) *chimie douce* (soft chemical) synthesis, (2) solvothermal methods, and (3) high-temperature solid-state reactions. MoS_2 nanoclusters have been

* Corresponding author at: Department of Chemistry, Northwestern University, 2145 Sheridan Road, Evanston, IL 60208, USA. Fax: +1 847 491 7713.
E-mail address: todom@northwestern.edu (T.W. Odom).
[1] Present address: Green Earth Technologies, Inc., 863 Mitten Road, Burlingame, CA 94010, USA.

0022-4596/$ - see front matter © 2008 Elsevier Inc. All rights reserved.
doi:10.1016/j.jssc.2008.06.004

synthesized within inverse micelles [11], and MoS_2, $MoSe_2$, WS_2 and WSe_2 nanoparticles have been grown starting from transition metal (*M*) carbonyl and chalcogen (*E*) precursors [33]. Nanoparticles produced using solution-based methods, however, are generally amorphous and require further annealing treatments to improve crystallinity. Although solvothermal methods can produce improved crystalline materials compared to *chimie douce* processes, a challenge is size control [34–37]. An advantage is that a variety of binary (e.g. $NiSe_2$, $CoSe_2$) and ternary metal chalcogenides (e.g. Ag_8SnS_6, and Ag_8SnSe_6) can easily be grown using solvothermal chemistry [38–41]. Under high-temperature conditions, inorganic fullerene-like nanoparticles and multi-walled inorganic nanotubes have been produced, such as WS_2 nanotubes starting from WO_{3-x} particles [42] and MoS_2, WS_2, and $MoSe_2$ particles and nanotubes from the decomposition of ammonia salts ($(NH_4)_2ME_4$) or metal trichalcogenides (ME_3) [43–47]. None of these methods, however, can facilitate the assembly of nanoscale TMC materials into specific locations on a substrate. Such control is critical for investigation of their properties at the single nanostructure level and also for direct integration into devices. Early efforts for organizing MoS_2 nanowires have used the step edges of a graphite surface as a template [48,49], although the structures are usually transferred to a different substrate for chemical sensing and other applications.

2. Introduction to methodologies

Our work has focused on expanding the strategies for creating nanoscale TMC materials beyond semiconductors and has explored unique approaches for producing TMCs based on refractory metals. Moreover, these nanomaterials can be grown in ordered arrays, with sizes that are easily tunable, and with unusual but controllable shapes. We have carried out solid-state reactions *on surfaces*, where patterned arrays of metal nanostructures are chemically transformed [50–52], and *in beakers*, where molecular precursors are decomposed in a one-pot synthesis [53].

Fig. 1A outlines how solid-state reactions can occur on a substrate patterned with metal nanostructures. First, phase shifting photolithography (PSP) with a *hard*-PDMS (polydimethylsiloxane) mask is used to generate sub-250 nm trenches in a negative tone photoresist [54]. After metal deposition and removal of the photoresist template, metal nanostructures are patterned and chemically converted into their metal chalcogenide by heating the substrate in a quartz tube furnace in the presence of H_2S gas or Se vapor sublimed from Se powder. In general, refractory metals (Ta and Mo) required much higher temperatures ($>850\,^{\circ}C$) for chemical transformation compared to softer metals (Ni and Ag), where temperatures were less than $400\,^{\circ}C$.

Fig. 1B depicts our one-pot approach to synthesize *metallic* TMC nanomaterials. First, the appropriate molecular precursors (usually $NbCl_5$ or $TaCl_5$), chalcogen sources (Se, Na_2S, or S), and amine surfactants were combined under nitrogen into a three-necked flask. This mixture was vigorously stirred at elevated temperatures ($>250\,^{\circ}C$) for several hours to form a black suspension. The amorphous intermediates were then extracted and washed with organic solvents (hexanes or ethanol) prior to a second high-temperature annealing step to achieve crystalline nanostructures [53]. In this procedure, the surfactant also served as the solvent, and the relative concentrations of these were critical for achieving shape and dimensionality control. The remaining sections of this paper will focus on specific examples of our work that highlight the novelty, versatility and flexibility of the two approaches.

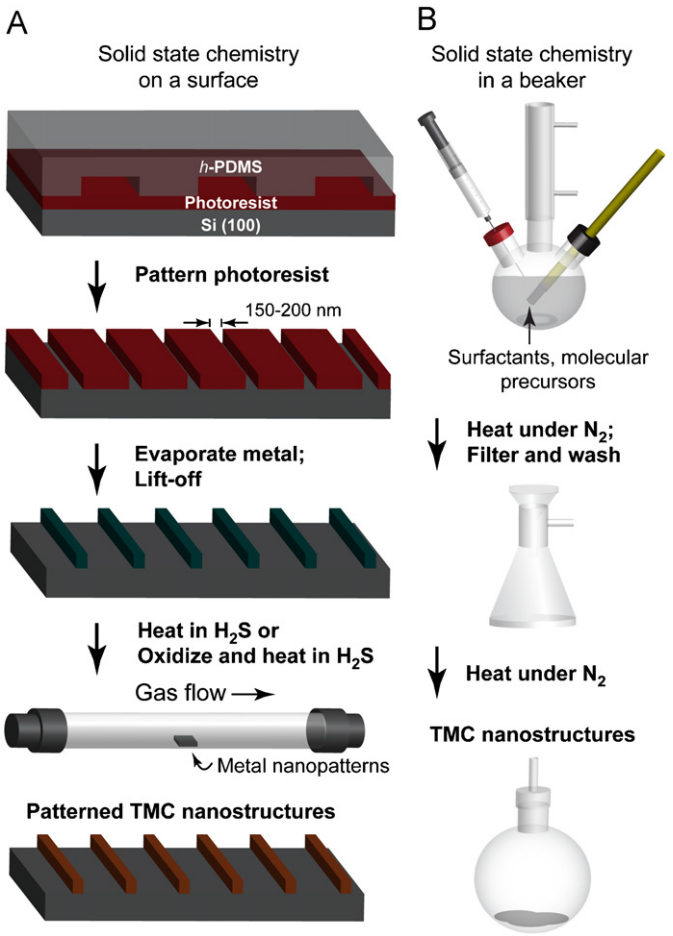

Fig. 1. (A) Scheme of the chemical nanofabrication procedure to generate patterned arrays of nanoscale transition metal chalcogenide (TMC) materials and (B) scheme of the one-pot, soft chemical synthesis of TMC nanostructures.

3. Solid-state chemistry on surfaces

3.1. Transition metal sulfide nanomaterials

Thin films of TMC materials have been prepared by a variety of methods, ranging from sequential deposition of constituent materials followed by annealing [55] to wet deposition from single-source precursors [56] to chemical vapor deposition [57]. From these precedents, we optimized our chemical transformation conditions by converting e-beam deposited thin metal films to their crystalline TMC analogues by heating the metal substrates in a quartz tube furnace under H_2S gas. For example, to create MoS_2 films, we heated thin films of Mo under $850\,^{\circ}C$ in the presence of Ar/H_2S for 4 h and discovered that the overall sizes of the crystals scaled with the thickness of the Mo film. In addition, patterned microscale structures (ca. 1 μm or larger) of Mo exhibited polycrystalline structures similar to those in the films.

To test whether reducing the sizes of the Mo patterns to nanoscale dimensions would make a difference, we patterned surfaces with sub-250 nm features. A thin (3–5 nm) adhesion layer of Cr was used to keep the Mo nanopatterns on the substrate. The chemical conversion conditions were identical to those described above for unpatterned Mo films. Interestingly, we observed that the relative orientation of the MoS_2 crystals could be controlled simply by altering the location of the nanopatterned Mo substrate within a quartz tube furnace (total length = 13″) [51]. Fig. 2A shows patterned MoS_2-lines where the *c*-axes of the

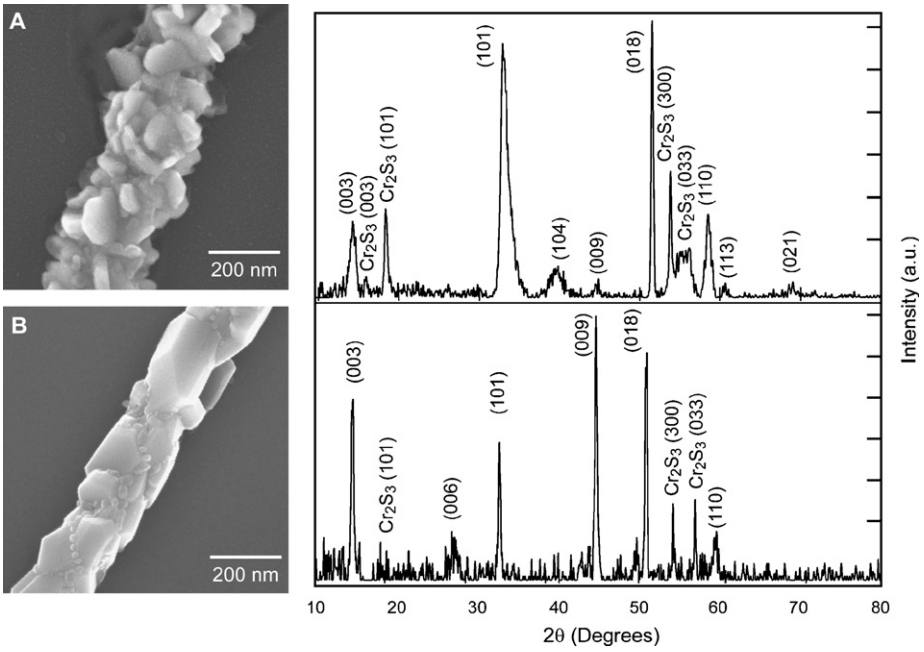

Fig. 2. Scanning electron microscopy (SEM) images and glancing angle X-ray diffraction (GAXD) spectra of patterned MoS_2 lines with nanocrystals whose *c*-axes are primarily oriented (A) perpendicular to the substrate and (B) parallel to the substrate. Adapted from Ref. [51].

MoS_2 nanocrystals are oriented roughly parallel to the substrate (the plates are on their edges); this morphology was formed at distances 3–4″ downstream from the furnace entrance. Fig. 2B shows MoS_2 crystals oriented where the *c*-axes are mostly perpendicular to the substrate; this orientation was formed 9–10″ downstream from the entrance. If the features of the patterned Mo were larger than 250 nm, no preferential orientation was observed. MoS_2 can exhibit three different polytypes: 2H-MoS_2 (hexagonal), 3R-MoS_2 (rhombohedral), 1T-TaS_2 (tetragonal) [49]. We used glancing angle X-ray diffraction (GAXD) to characterize the crystal structure of the patterned nanostructures in order to preserve their integrity on the surface. Comparison of the diffractograms indicated that the relative intensities of the peaks, especially those along the (00*l*) direction, verified the different crystal orientations imaged using SEM. The observed Cr_2S_3 peaks can be attributed to conversion of the Cr adhesion layer. Under our conditions, we observed only the 3R polytype.

To demonstrate the versatility of our chemical transformation approach to pattern other TMC nanomaterials, we generated a wide range of materials starting from different metals [52]. Fig. 3A shows a portion of a large area ($>1\,in^2$) array of NiS_2-lines patterned on a 400 nm pitch. Interestingly, the nanocrystals within these lines appear to overlap, and indeed, Fig. 3B confirms that the orientation of the nanocrystals follows the curve and direction of the metal template. GAXD spectra were consistent with bulk cubic NiS_2 (*Pa*−3, PDF #01-089-3058) (Fig. 3C). In general, we observed that TMC materials with higher symmetries (such as NiS_2, Ag_2S and Ag_2Se) tended to form more interconnected crystals than layered compounds like MoS_2 (Fig. 2) [52].

Because the NiS_2 nanocrystals were connected within the patterned structures, we could also generate free-standing structures. Here, we modified the nanopatterning method but kept the chemical transformation conditions the same. Fig. 4 outlines the procedure to generate NiS_2 rings: (1) PSP is used to define the overall shape in positive tone photoresist on Si (100) substrates; (2) Cr is deposited and then lifted-off to form slots in the Cr film, which acts as an etch mask; (3) the patterned substrate is anisotropically etched to form v-grooves in the Si into which Ni is deposited by e-beam (Cr mask is then removed); and

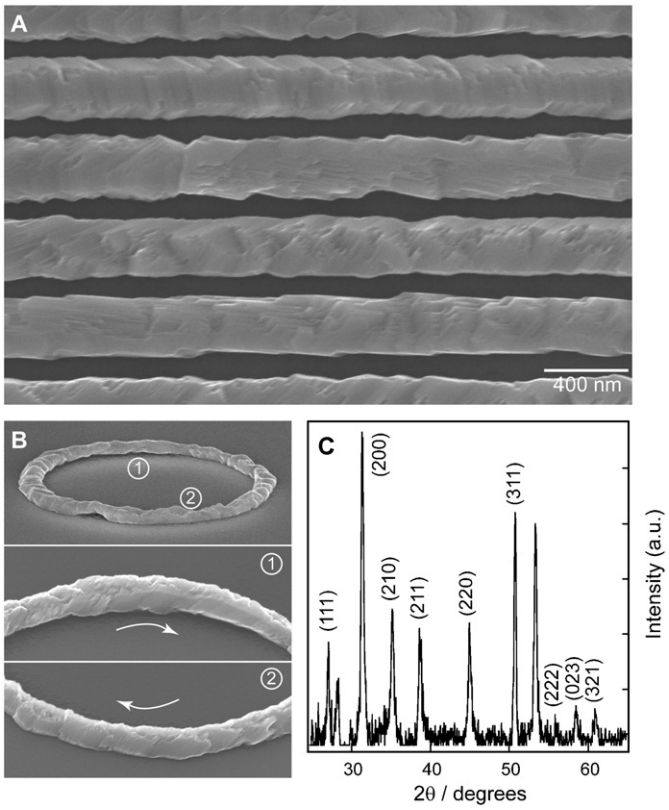

Fig. 3. (A) SEM image of nanoscale NiS_2 lines generated on a 400 nm pitch and (B) SEM image of NiS_2 rings. The tilt angle is 45°. The zoomed-in areas depict how nanocrystals within a NiS_2 ring overlap with each other and follow the curved direction of the pattern. (C) GAXD spectrum of nanopatterned NiS_2 lines exhibiting characteristic diffraction peaks for cubic NiS_2. Adapted from Ref. [52].

(4) the Ni is converted to NiS_2 and then released from the Si template [52]. These NiS_2 nanostructures can be dispersed into solution or transferred to a variety of substrates.

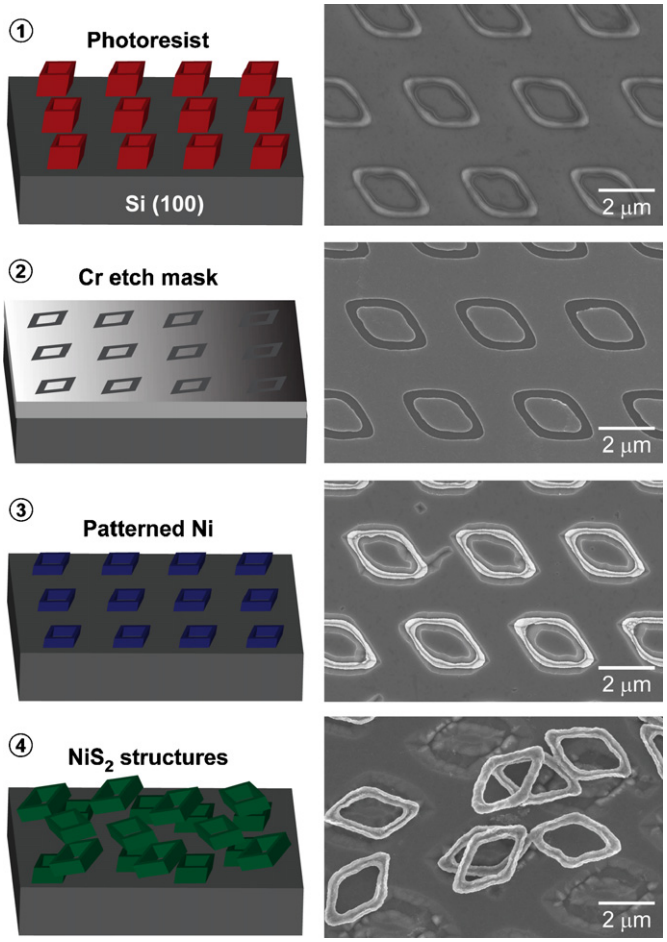

Fig. 4. Scheme and corresponding SEM images of the steps for generating free-standing NiS_2 nanostructures: (1) pattern-positive tone photoresist; (2) deposit Cr, lift-off, and then etch Si through Cr mask; (3) deposit Ni within etched Si and remove the Cr and (4) react with H_2S gas and then release from Si template.

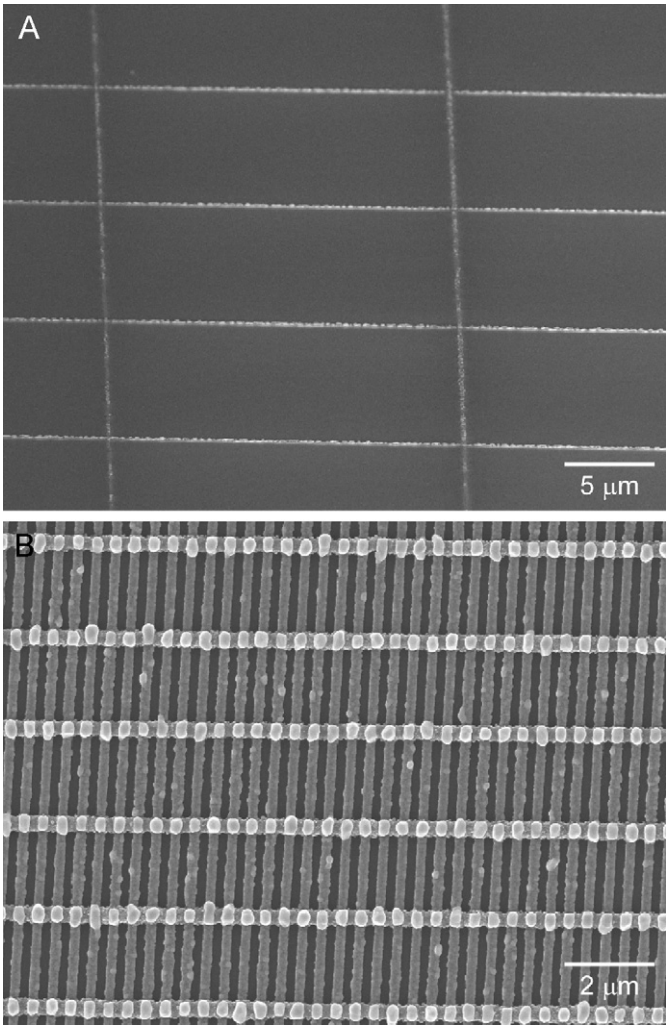

Fig. 5. SEM images of (A) Ag_2Se crossed line arrays (pitch: 10 μm × 25 μm) and (B) NiS_2 lines crossed with Ag_2Se lines (pitch: 400 nm × 2 μm). Adapted from Ref. [52].

3.2. Patterned mixed metal chalcogenide nanomaterials

The robustness of the patterned metal chalcogenide nanostructures enables us to generate crossed arrays out of the same as well as different materials. In the former case, the patterning is trivial as long as the metal templates can withstand multiple photolithographic steps. In the latter case, care must be taken when selecting the first patterned TMC nanomaterial so that it can handle the subsequent photolithography steps (processing of the next metal) as well as the second chemical conversion reaction.

Besides the ability to create metal sulfide nanomaterials, chemical nanofabrication can also produce metal selenide nanostructures. Fig. 5A depicts a crossed array of Ag_2Se lines that overlap other Ag_2Se lines that were made from crossed Ag lines that were converted in the presence of Se vapor (~8 mTorr at 200 °C). We demonstrated that arrays of NiS_2 lines crossed with Ag_2Se lines could be generated (Fig. 5B). Here NiS_2 was patterned first because it was stable at the lower reaction temperatures used for the conversion of Ag to Ag_2Se. Although neither Ag_2Se nor Ag_2S nanostructures appeared to exhibit nanocrystalline structure (patterned lines appeared smooth), GAXD identified crystalline planes [52].

3.3. Tantalum oxide and tantalum sulfide nanomaterials

Although we have highlighted the advantages of this chemical conversion approach to generate TMC nanomaterials, there are two potential limitations: (1) the metal deposited by e-beam must not damage the photoresist template and (2) the substrate supporting the metal nanopatterns must not react with the chalcogen source. The former is problematic primarily for refractory metals (such as Ta, Nb, and Mo), which can cause significant heating of the e-beam chamber during deposition. The elevated temperatures cause the photoresist polymer to cross-link, and standard lift-off in organic solvents cannot be easily used to produce the metal nanopatterns. We overcame this challenge by first exposing the photoresist to an oxygen plasma and then sonicating the substrate in water. Ta nanopatterns were fabricated using this modified approach to lift-off and then subjected to typical sulfidization conditions in the tube furnace. In contrast to the Mo system, which could be converted directly to MoS_2 from the as-deposited Mo nanopatterns, the Ta patterns did not converted to TaS_2 without an intermediate oxidation step.

Not surprisingly, we found that the oxidation temperature (650–850 °C) had a significant impact on the crystallinity and morphology of the tantalum oxide (Fig. 6). As the temperature increased from 650 to 750 °C, the characteristic peaks of orthorhombic Ta_2O_5 (*Pmm*2, PDF #00-025-0922) increased in intensity while the FWHM decreased. Such changes are characteristic of improved crystallinity, although no marked differences in morphology were observed in SEM images (Fig. 6, insets). Under an increased oxidation temperature of 850 °C, the Ta_2O_5

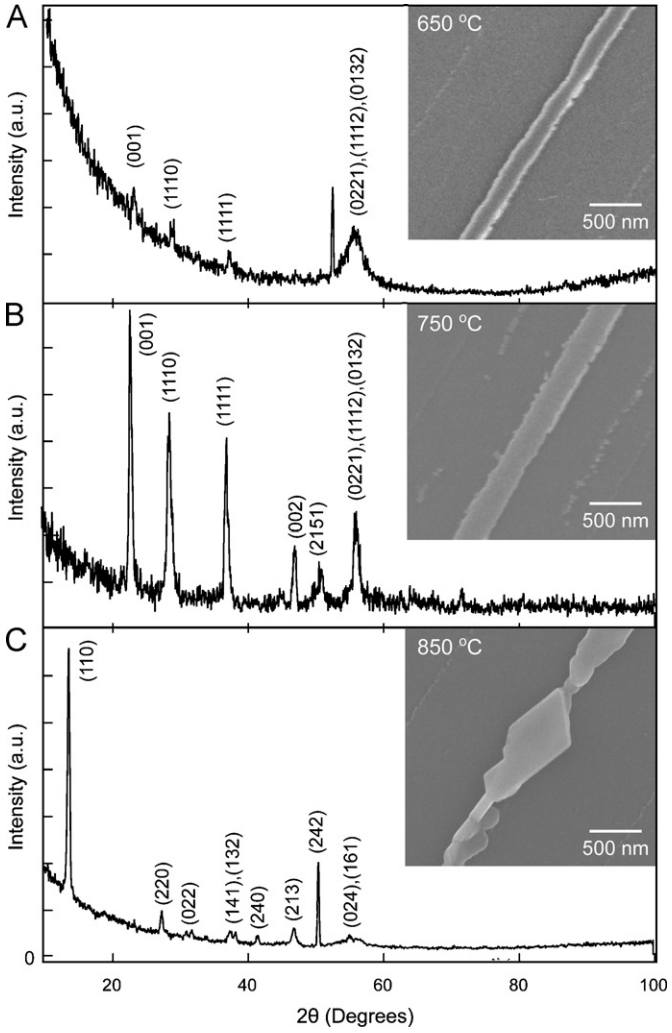

Fig. 6. GAXD spectra and SEM images of lines of (A) nearly amorphous Ta_2O_5 oxidized at 650 °C, (B) crystalline Ta_2O_5 oxidized at 750 °C, and (C) Ta_2O_5 oxidized at 850 °C. Note that (B) and (C) exhibit different crystal structures.

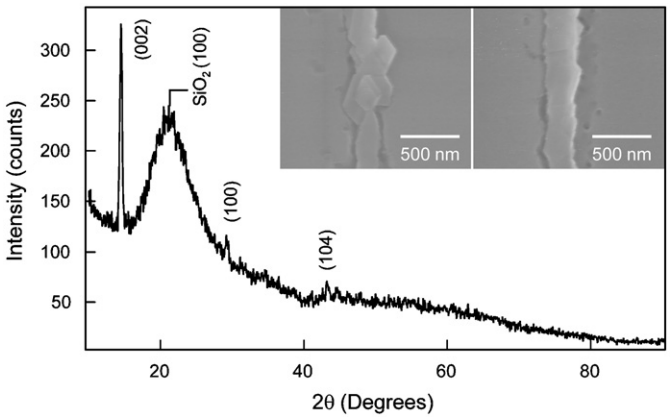

Fig. 7. GAXD spectra and SEM images (insets) of near perfectly oriented TaS_2 lines with the *c*-axis perpendicular to the substrate.

lines were faceted and adopted an alternate orthorhombic structure (*Ibam*, PDF#00-054-0514). The lateral dimensions increased from ~225 to ~280 nm.

Fig. 7 shows crystalline TaS_2 structures obtained after heating polycrystalline Ta_2O_5 (650 °C) in H_2S at ~3 Torr at 950 °C. We observed that using the oxides generated at lower temperatures yielded more continuous TaS_2 nanopatterns than those from more crystalline Ta_2O_5 materials (850 °C). Similar to 2H-MoS_2, 2H-TaS_2 is a layered material with Ta atoms sandwiched between two layers of trigonally coordinated S atoms. It is noteworthy that the TaS_2 lines were oriented near perfectly with the *c*-axis perpendicular to the fused silica substrate. The intense and narrow (002) peak along with the weak (101) and (104) peaks in the GAXD spectra (*P*63/*mmc*, PDF#01-080-0685) verified the crystal orientation relative to the substrate. We attribute the broad peak at ~22° to the polycrystalline silica substrate (the (100) peak is at 22.4°, PDF#01-070-3315). Some etching of the fused silica was also observed under the TaS_2 nanostructures after the reaction.

4. One-pot synthesis of metallic TMC nanomaterials

As an alternative approach for controlling the crystal structure, size, and shapes of TMC nanomaterials, we have also pursued synthetic methods to grow layered, *conducting* ME_2 nanostructures. We have focused primarily on TaS_2 and $NbSe_2$ [53] because these materials exhibit correlated electron phenomena, such as superconductivity and CDW behavior. Using a one-pot synthesis, we have developed procedures to generate 2D nanomaterials out of TaS_2, $TaSe_2$ and $NbSe_2$ and 1D nanomaterials from $NbSe_2$. The key for obtaining different dimensionalities was the relative amount of surfactant (typically an amine) that stabilized the chalcogen-rich (001) planes. Although quantification of the absolute amounts of surfactant on the crystals was difficult to determine, we could qualitatively tune the relative concentrations of surfactant to ME_2 material to control dimensionality.

$TaSe_2$ and TaS_2 nanomaterials were synthesized following the outline in Fig. 1B [53] to form nanoplates with thicknesses between 15 and 60 nm and lateral dimensions between 300 and 800 nm (Fig. 8). In brief, $TaCl_5$, elemental Se and dodecylamine were combined under N_2 to form a black suspension of precursor materials. After heating to 250 °C for 4 h and stirring vigorously, the intermediate was extracted and washed repeatedly with hexane, dried under vacuum, and then heated at 650 °C in a quartz reaction flask for another 4 h under N_2. TaS_2 nanoplates were synthesized by the same general procedure except substituting solid S for Se, heating the intermediate to 250 °C for 2 h, and annealing at 650 °C for 2 h under N_2. We found that crystalline products were not obtained if the intermediate was annealed at lower temperatures (<550 °C) or for shorter reaction times (<2 h). In addition, we found that the relative amount of surfactant at each step played an important role in the formation of the nanoplates, which might explain why $TaSe_2$ or TaS_2 nanoplates were not generated if the intermediates were extracted with ethanol instead of hexane.

Powder X-ray diffraction (PXRD) patterns of TaS_2 and $TaSe_2$ nanoplates were consistent with bulk 2H-$TaSe_2$ (PDF#01-73-1799) and 2H-TaS_2 (PDF #01-80-0685) (Fig. 8, insets). The peaks of the $TaSe_2$ and TaS_2 nanostructures were broad, and the increased full width half max of the (002) peak in the XRD pattern indicates a decreased number of layers along the *c*-axis. In contrast to the surface-patterned, chemical transformation method to TaS_2 nanomaterials (Fig. 7), the one-pot synthesis did not exhibit well-faceted edges. Both the solution synthesis and the nanofabrication approaches, however, produced the same hexagonal crystal structure (*P*63/*mmc*), although the temperatures required to produce the TaS_2 nanomaterials were different. In the *chimie douce* approach, 2D crystals were grown at 650 °C from Ta

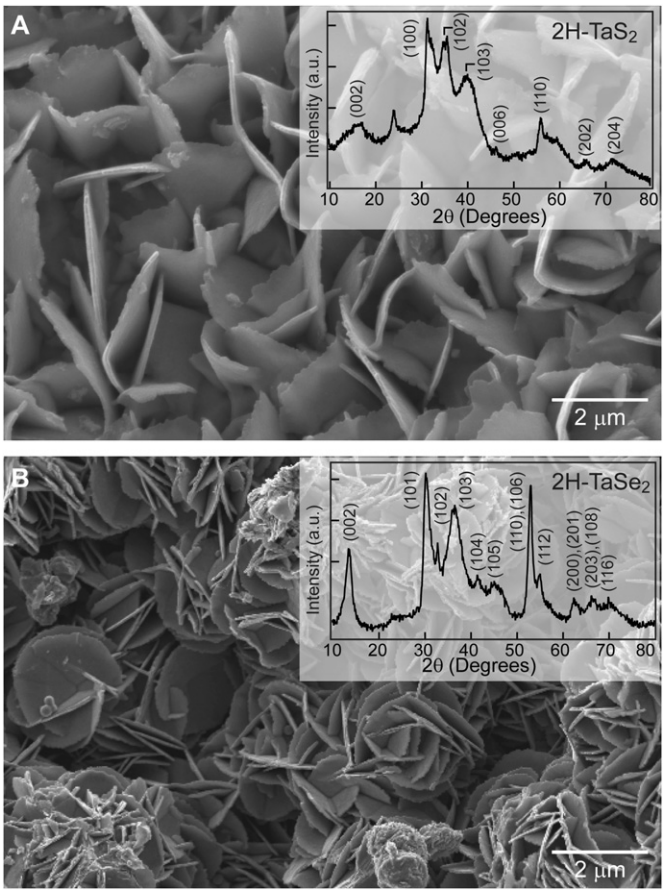

Fig. 8. SEM images and PXRD patterns (insets) of a one-pot chemical synthesis of (A) TaS_2 nanoplates and (B) $TaSe_2$ nanoplates.

precursors and surfactants, although no conversion was observed from the nanopatterned Ta_2O_5 structures until 950 °C.

Using reaction conditions similar to those for TaS_2 and $TaSe_2$, we have also synthesized $NbSe_2$ nanoplates and nanowires. The primary difference for the niobium system was that the annealing step occurred at a lower temperature, 450 °C. Nanoscale $NbSe_2$ formed different morphologies depending on the washing temperature of the intermediate. When the reaction mixture was cooled to room temperature slowly (~5 °C/min) before washing with hexane, 2D lamellar plates were achieved (Fig. 9A). The thicknesses of the nanoplates ranged from 10 to 70 nm and the lateral dimensions ranged from 500 to 1000 nm. In contrast, when the black suspension was quenched rapidly with room-temperature hexane, 1D nanowires were formed (Fig. 9B). The $NbSe_2$ nanowires were tens of microns long and between 2 and 25 nm in diameter. High-resolution transmission electron microscopy (HRTEM) images revealed that individual nanowires were polycrystalline and that the wires grew perpendicular to the (002) direction [53]. The selected area electron diffraction (SAED) pattern of several (3–5) nanowires exhibited slightly broadened diffraction spots because occasionally the stacked $NbSe_2$ sheets in the nanowires were not uniformly spaced along the length of the wire. PXRD of the 2D and 1D-structures were consistent with 2H-$NbSe_2$ (PDF#19-0872).

5. Concluding remarks

TMC nanomaterials can be generated on surfaces and in beakers with control over their size, shape, and crystal structure.

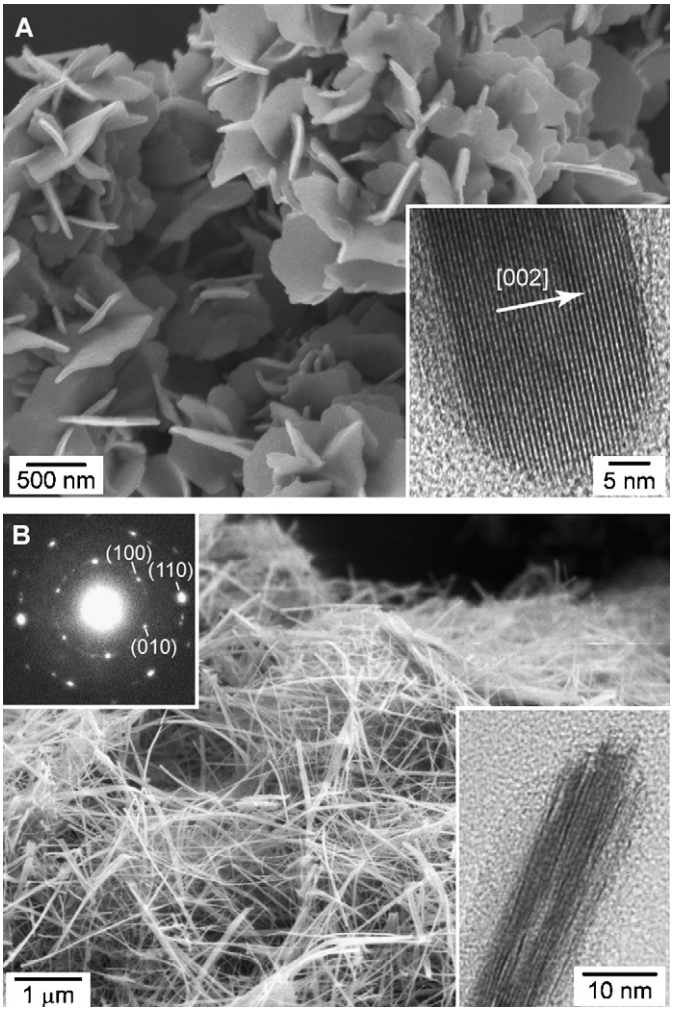

Fig. 9. SEM images of (A) 2D nanoscale $NbSe_2$ plates. Inset shows a HRTEM image of an individual nanoplate on its edge. (B) 1D nanoscale $NbSe_2$ wires. Top inset shows a SAED pattern of a small number of nanowires. Bottom inset depicts a HRTEM image of an 8.8-nm nanowire. Adapted from Ref. [53].

Such flexibility offered by chemical nanofabrication and soft chemical methods opens new possibilities to study finite-size effects, especially as a function of well-controlled sizes, on correlated electron phenomena in TaS_2 and $NbSe_2$. Moreover, TMC materials patterned over multiple length scales can enhance applications where large surface areas are important, such as in chemical sensing and catalysis. Because multiple, different TMC nanomaterials can now be easily patterned on a single substrate, opportunities for multiplexed sensing and broadband absorption for photovoltaics can also be envisioned. Moreover, we anticipate that these new types of patterned and crystalline nanomaterials will enable unique prospects for interrogating solid solutions and solid-state chemical reactions at the nanoscale.

Acknowledgments

This research was supported by an NSF CAREER Award (CHE-0349302). This work made use of the NU*ANCE* Center facilities and the J.B. Cohen X-ray Diffraction Facility, which are supported by NSF-NSEC, NSF-MRSEC, and the Keck Foundation at Northwestern University. T.W.O. is a DuPont Young Professor, an Alfred P. Sloan Research Fellow, a Cottrell Scholar of Research Corporation, and a David and Lucile Packard Fellow.

References

[1] R.S. Mane, C.D. Lokhande, Mater. Chem. Phys. 65 (2000) 1.
[2] S.K. Sharma, S. Kumar, V. Kumar, T.P. Sharma, Opt. Mater. 13 (1999) 261.
[3] M. Kouzu, K. Uchida, Y. Kuriki, F. Ikazaki, Appl. Catal. A 276 (2004) 241.
[4] O. Solorza-Feria, K. Ellmer, M. Giersig, N. Alonso-Vante, Electrochim. Acta 39 (1994) 1647.
[5] L. Rapoport, V. Leshchinsky, Y. Volovik, M. Lvovsky, O. Nepomnyashchy, Y. Feldman, R. Popovitz-Biro, R. Tenne, Surf. Coatings Technol. 163–164 (2003) 405.
[6] I.L. Singer, S. Fayeulle, P.D. Ehni, Wear 195 (1996) 7.
[7] C. Liang, K. Terabe, T. Hasegawa, M. Aono, Solid State Ionics 177 (2006) 2527.
[8] I. Rom, W. Sitte, Solid State Ionics 101–103 (1997) 381.
[9] N. Barreau, J.C. Bernede, J. Phys. D: Appl. Phys. 35 (2002) 1197.
[10] P.G. Moses, B. Hinnemann, H. Topsoe, J.K. Norskov, J. Catal. 248 (2007) 188.
[11] J.P. Wilcoxon, J. Phys. Chem. B 104 (2000) 7334.
[12] R. Dominko, M. Gaberscek, D. Arcon, A. Mrzel, M. Remskar, D. Mihailovic, S. Pejovnik, J. Jamnik, Electrochim. Acta 48 (2003) 3079.
[13] R. Tenne, J. Mater. Res. 21 (2006) 2726.
[14] M. Nath, C.N.R. Rao, Pure Appl. Chem. 74 (2002) 1545.
[15] L. Rapoport, Y. Bilik, Y. Feldman, M. Homyonfer, S.R. Cohen, R. Tenne, Nature 387 (1997) 791.
[16] M. Chhowalla, G. Amaratunga, Nature 407 (2000) 164.
[17] W. Xingcai, T. Yourong, H. Yeming, Y. Song, H. Zheng, Z. Jungjie, L. Dong, Nanotechnology 17 (2006) 201.
[18] R. Laiho, M. Safonchik, K.B. Traito, Phys. Rev. B: Condens. Matter Mater. Phys. 75 (2007) 174524.
[19] A. Falk, M.M. Deshmukh, A.L. Prieto, J.J. Urban, A. Jonas, H. Park, Phys. Rev. B: Condens. Matter Mater. Phys. 75 (2007) 020501.
[20] Z. Zhou, R. Jin, G. Eres, D. Mandrus, V. Barzykin, P. Schlottmann, Y.S. Hor, Z. Xiao, J.F. Mitchell, Phys. Rev. B: Condens. Matter Mater. Phys. 76 (2007) 104511.
[21] R.F. Frindt, Phys. Rev. Lett. 28 (1972) 299.
[22] M. Nath, S. Kar, A.K. Raychaudhuri, C.N.R. Rao, Chem. Phys. Lett. 368 (2003) 690.
[23] C.W. Dunnill, H.K. Edwards, P.D. Brown, D.H. Gregory, Angew. Chem. Int. Ed. 45 (2006) 7060.
[24] V.Ya. Pokrovskii, S.G. Zybtsev, I.G. Gorlova, Phys. Rev. Lett. 98 (2007) 206404.
[25] A.P. Orlov, Y.I. Latyshev, A.M. Smolovich, P. Monceau, JETP Lett. 84 (2006) 89.
[26] T. Toshima, S. Tanda, Physica C: Superconductivity 426–431 (2005) 426.
[27] Y.S. Hor, Z.L. Xiao, U. Welp, Y. Ito, J.F. Mitchell, R.E. Cook, W.K. Kwok, G.W. Crabtree, Nano Lett. 5 (2005) 397.
[28] E. Slot, M.A. Holst, H.S.J. van der Zant, S.V. Zaitsev-Zotov, Phys. Rev. Lett. 93 (2004) 176602.
[29] S.V. Zaitsev-Zotov, V.E. Minakova, Phys. Rev. Lett. 97 (2006) 266404.
[30] Y.S. Hor, U. Welp, Y. Ito, Z.L. Xiao, U. Patel, J.F. Mitchell, W.K. Kwok, G.W. Crabtree, Appl. Phys. Lett. 87 (2005) 142506.
[31] T. Toshima, K. Inagaki, N. Hatakenaka, S. Tanda, J. Phys. Soc. Jpn. 75 (2006) 24706.
[32] Z. Zhixian, J. Rongying, E. Gyula, M. David, B. Victor, S. Pedro, H. Yew-San, X. Zhili, F.M. John, Phys. Rev. B (Condens. Matter Mater. Phys.) 76 (2007) 104511.
[33] D. Duphil, S. Bastide, J.C. Rouchaud, J.L. Pastol, B. Legendre, C. Levy-Clement, Nanotechnology 15 (2004) 828.
[34] X. Cao, Q. Lu, X. Xu, J. Yan, H. Zeng, Mater. Lett. 62 (2008) 2567.
[35] X. Wang, F. Wan, Y. Gao, J. Liu, K. Jiang, J. Cryst. Growth 310 (2008) 2569.
[36] B. Subhajit, K. Soumitra, Nanotechnology (2008) 045710.
[37] Z. Nan, X.-Y. Wang, Z. Zhao, J. Cryst. Growth 295 (2006) 92.
[38] S. Jana, I.C. Baek, M.A. Lim, S.I. Seok, J. Colloid Interface Sci. 322 (2008) 473.
[39] Q. Li, Y. Ding, X. Liu, Y. Qian, Mater. Res. Bull. 36 (2001) 2649.
[40] Y. Xie, H. Su, B. Li, Y. Qian, Mater. Res. Bull. 35 (2000) 459.
[41] J. Yang, G.H. Cheng, J.H. Zeng, S.H. Yu, X.M. Liu, Y.T. Qian, Chem. Mater. 13 (2001) 848.
[42] A. Rothchild, S.R. Cohen, R. Tenne, Appl. Phys. Lett. 75 (1999) 4025.
[43] C.N.R. Rao, Int. J. Nanosci. 4 (2005) 811.
[44] N. Manashi, C.N.R. Rao, J. Am. Chem. Soc. 123 (2001) 4841.
[45] Y. Feldman, G.L. Frey, M. Homyonfer, V. Lyakhovitskaya, A. Margolin, S.R. Cohen, G. Hodes, J.L. Hutchison, R. Tenne, J. Am. Chem. Soc. 118 (1996).
[46] A. Margolin, R. Popovitz-Biro, A. Alby-Yaron, L. Rapoport, R. Tenne, Chem. Phys. Lett. 411 (2005) 162.
[47] C. Schuffenhauer, R. Popovitz-Biro, R. Tenne, J. Mater. Chem. 12 (2002) 1587.
[48] Q. Li, J.T. Newbarg, E.C. Walter, J.C. Hemminger, R.M. Penner, Nano Lett. 4 (2004) 277.
[49] Q. Li, E.C. Walter, W.E.v.d. Veer, B.J. Murrey, J.T. Newberg, E.W. Bohannan, J.A. Switzer, J.C. Hemminger, R.M. Penner, J. Phys. Chem. B 109 (2005) 3169.
[50] J. Henzie, J.E. Barton, C.L. Stender, T.W. Odom, Acc. Chem. Res. 39 (2006) 249.
[51] C.L. Stender, E.C. Greyson, Y. Babayan, T.W. Odom, Adv. Mater. 17 (2005) 2837.
[52] C.L. Stender, T.W. Odom, J. Mater. Chem. 17 (2007) 1866.
[53] P. Sekar, E.C. Greyson, J.E. Barton, T.W. Odom, J. Am. Chem. Soc. 127 (2005) 2054.
[54] T.W. Odom, V.R. Thalladi, J.C. Love, G.M. Whitesides, J. Am. Chem. Soc. 124 (2002) 12112.
[55] C. Amory, J.C. Bernede, N. Hamdadou, Vacuum 72 (2004) 351.
[56] P. Roy, S.K. Srivastava, Thin Solid Films 496 (2006) 293.
[57] A. Jager-Waldau, M. Lux-Steiner, R. Jager-Waldau, R. Burkhardt, E. Bucher, Thin Solid Films 189 (1990) 339.